

# $1\alpha,25(\text{OH})_2$ -3-Epi-Vitamin $\text{D}_3$ , a Natural Physiological Metabolite of Vitamin $\text{D}_3$ : Its Synthesis, Biological Activity and Crystal Structure with Its Receptor

Ferdinand Molnár<sup>1,2</sup>, Rita Sigüeiro<sup>3</sup>, Yoshiteru Sato<sup>1</sup>, Clarisse Araujo<sup>3</sup>, Inge Schuster<sup>4</sup>, Pierre Antony<sup>1</sup>, Jean Peluso<sup>5</sup>, Christian Muller<sup>5</sup>, Antonio Mouriño<sup>3</sup>, Dino Moras<sup>1</sup>, Natacha Rochel<sup>1\*</sup>

**1** Institut de Génétique et de Biologie Moléculaire et Cellulaire (IGBMC), Institut National de Santé et de Recherche Médicale (INSERM) U964/Centre National de Recherche Scientifique (CNRS) UMR 7104/Université de Strasbourg, Illkirch, France, **2** School of Pharmacy, Faculty of Health Sciences, University of Eastern Finland, Kuopio, Finland, **3** Departamento de Química Orgánica, Universidad de Santiago de Compostela and Unidad Asociada al CSIC, Santiago de Compostela, Spain, **4** Institute of Pharmaceutical Chemistry, University of Vienna, Vienna, Austria, **5** Faculty of Pharmacy, Institut Gilbert Laustriat, UMR 7175 CNRS, University of Strasbourg, Illkirch, France

## Abstract

**Background:** The  $1\alpha,25$ -dihydroxy-3-epi-vitamin- $\text{D}_3$  ( $1\alpha,25(\text{OH})_2$ -3-epi- $\text{D}_3$ ), a natural metabolite of the seco-steroid vitamin  $\text{D}_3$ , exerts its biological activity through binding to its cognate vitamin D nuclear receptor (VDR), a ligand dependent transcription regulator. *In vivo* action of  $1\alpha,25(\text{OH})_2$ -3-epi- $\text{D}_3$  is tissue-specific and exhibits lowest calcemic effect compared to that induced by  $1\alpha,25(\text{OH})_2\text{D}_3$ . To further unveil the structural mechanism and structure-activity relationships of  $1\alpha,25(\text{OH})_2$ -3-epi- $\text{D}_3$  and its receptor complex, we characterized some of its *in vitro* biological properties and solved its crystal structure complexed with human VDR ligand-binding domain (LBD).

**Methodology/Principal Findings:** In the present study, we report the more effective synthesis with fewer steps that provides higher yield of the 3-epimer of the  $1\alpha,25(\text{OH})_2\text{D}_3$ . We solved the crystal structure of its complex with the human VDR-LBD and found that this natural metabolite displays specific adaptation of the ligand-binding pocket, as the 3-epimer maintains the number of hydrogen bonds by an alternative water-mediated interaction to compensate the abolished interaction with Ser278. In addition, the biological activity of the  $1\alpha,25(\text{OH})_2$ -3-epi- $\text{D}_3$  in primary human keratinocytes and biochemical properties are comparable to  $1\alpha,25(\text{OH})_2\text{D}_3$ .

**Conclusions/Significance:** The physiological role of this pathway as the specific biological action of the 3-epimer remains unclear. However, its high metabolic stability together with its significant biologic activity makes this natural metabolite an interesting ligand for clinical applications. Our new findings contribute to a better understanding at molecular level how natural metabolites of  $1\alpha,25(\text{OH})_2\text{D}_3$  lead to significant activity in biological systems and we conclude that the C3-epimerization pathway produces an active metabolite with similar biochemical and biological properties to those of the  $1\alpha,25(\text{OH})_2\text{D}_3$ .

**Citation:** Molnár F, Sigüeiro R, Sato Y, Araujo C, Schuster I, et al. (2011)  $1\alpha,25(\text{OH})_2$ -3-Epi-Vitamin  $\text{D}_3$ , a Natural Physiological Metabolite of Vitamin  $\text{D}_3$ : Its Synthesis, Biological Activity and Crystal Structure with Its Receptor. PLoS ONE 6(3): e18124. doi:10.1371/journal.pone.0018124

**Editor:** Moray Campbell, Roswell Park Cancer Institute, United States of America

**Received:** October 24, 2010; **Accepted:** February 21, 2011; **Published:** March 31, 2011

**Copyright:** © 2011 Molnár et al. This is an open-access article distributed under the terms of the Creative Commons Attribution License, which permits unrestricted use, distribution, and reproduction in any medium, provided the original author and source are credited.

**Funding:** This study received financial support from CNRS, INSERM, ULP, the European Commission as SPINE2-complexes (contract no. LSHG-CT-2006-031220) under the RDT programme 'Quality of Life and Management of Living Resources', the Spanish Ministry of Education and Science (Grant SAF2007-67205) and Xunta de Galicia (Projects INCITE08PXIB-209130PR and ACEUIC-2006/XA050). Dishman-Netherlands provided the gift of vitamin  $\text{D}_2$ . R.S. thanks the Spanish MEC for a predoctoral fellowship. F.M. thanks the Academy of Finland for a postdoctoral fellowship (128226). The funders had no role in study design, data collection and analysis, decision to publish, or preparation of the manuscript.

**Competing Interests:** The authors have declared that no competing interests exist.

\* E-mail: rochel@igbmc.fr

## Introduction

The  $1\alpha,25$ -dihydroxyvitamin  $\text{D}_3$  ( $1\alpha,25(\text{OH})_2\text{D}_3$  or calcitriol), is the most active form of vitamin  $\text{D}_3$  and mediates its pleiotropic effects through VDR activation, which heterodimerizes with retinoid X receptor (RXR). VDR-induced genomic action results in growth inhibition of lymphomas, breast or prostate primary tumor cells, renal osteodystrophy, osteoporosis, psoriasis or autoimmune diseases [1,2]. Consequently, VDR is an exquisite therapeutic target to combat human metabolic diseases and uncontrolled cell proliferation in many tissues [3–5]. In addition  $1\alpha,25(\text{OH})_2\text{D}_3$  is a key regulator

of calcium and phosphate homeostasis and bone metabolism but its intrinsic hypercalcemic effect prevents its use in therapeutical applications [6].

$1\alpha,25(\text{OH})_2\text{D}_3$  is subjected to enzymatic inactivation via two major pathways leading to C-24 and C-23 hydroxylated metabolites in various tissues [7–17]. While the side chain oxidation is a general pathway associated to inactivation, another metabolite modified at the A-ring, the  $1\alpha,25(\text{OH})_2$ -3-epi- $\text{D}_3$ , has been shown to retain significant biological activity compared to the natural hormone [18,19]. The  $1\alpha,25(\text{OH})_2$ -3-epi- $\text{D}_3$  was initially identified in the culture of human neonatal keratinocytes [20,21]. Further *in vivo* studies have characterized the occurrence of a C-3

epimerization pathway [22]. Indeed, this natural vitamin  $\text{D}_3$  metabolite was detected in serum of rats treated with pharmacological doses of  $1\alpha,25(\text{OH})_2\text{D}_3$ , and may therefore play an important physiological role by buffering the level of  $1\alpha,25(\text{OH})_2\text{D}_3$ . In addition, significant accumulation of  $1\alpha,25(\text{OH})_2\text{-3-epi-D}_3$  was observed in different human adenocarcinoma cell lines such as

colon-derived Caco-2 cells [23] or NCI-H441 pulmonary cells [24]. Moreover,  $1\alpha,25(\text{OH})_2\text{-3-epi-D}_3$  was readily quantified in bovine parathyroid cells, [25] rat osteoblastic UMR 106 and Ros17/2.8 cells [26].

The production of  $1\alpha,25(\text{OH})_2\text{-3-epi-D}_3$  is initiated via A-ring C3-epimerization (Figure 1), where the C-3 hydroxyl moiety is

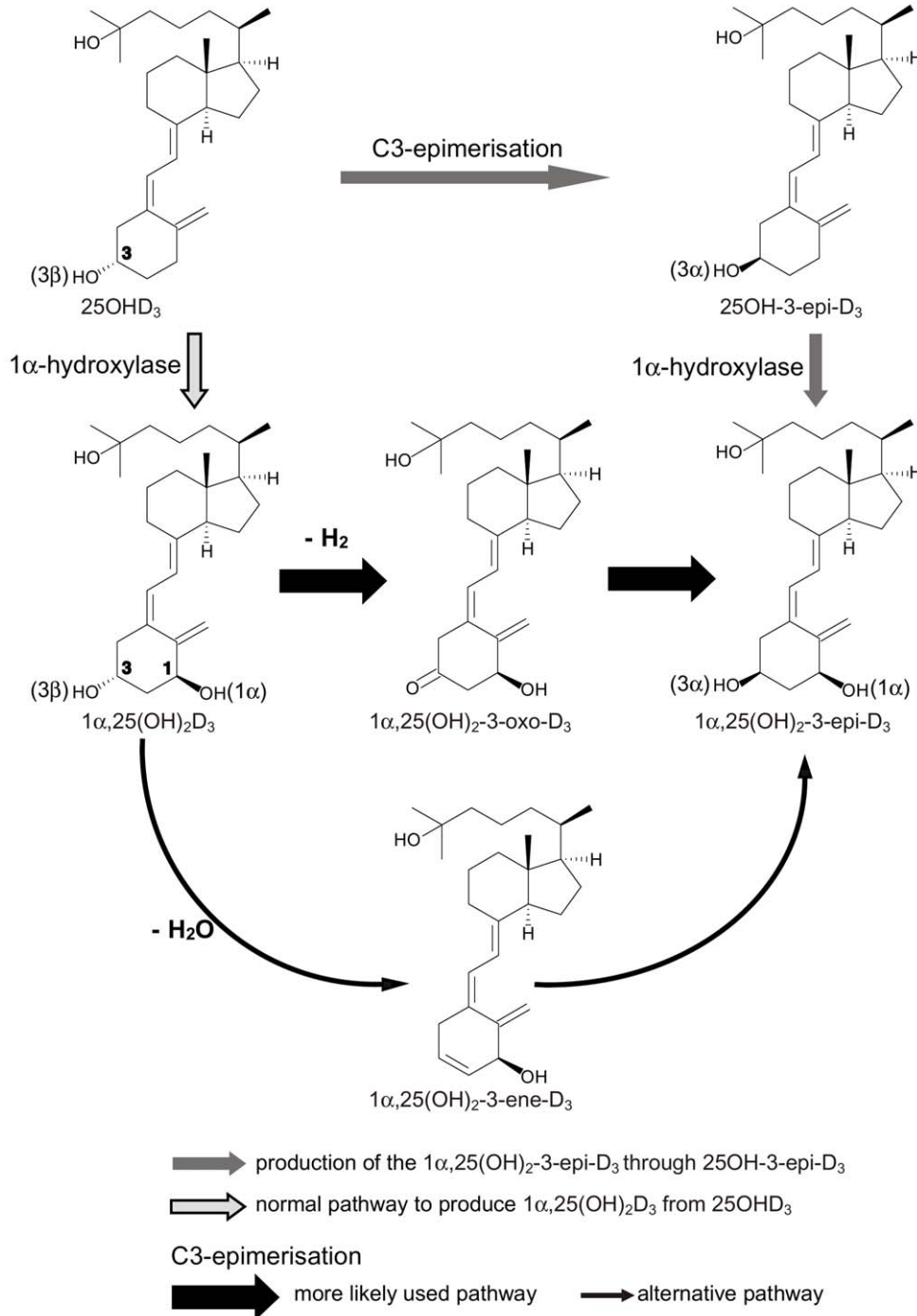


**Figure 1. Proposed pathway of the  $1\alpha,25(\text{OH})_2\text{-3-epi-D}_3$  production [18].** The reaction is initiated via A-ring C3-epimerization, where the C-3 hydroxyl moiety is changed from  $\beta$  to its diastereomer  $\alpha$ . Two distinct pathways may be employed by cells to generate  $1\alpha,25(\text{OH})_2\text{-3-epi-D}_3$ . The first, more likely used pathway, starts with dehydrogenation catalyzed by yet unidentified enzyme leading to a keto-intermediate, which is converted most probably by the same enzyme to the final product  $1\alpha,25(\text{OH})_2\text{-3-epi-D}_3$ . The second one uses dehydration and a subsequent hydroxylation at C-3  $\alpha$  position.

doi:10.1371/journal.pone.0018124.g001

changed from position  $\beta$  to its diastereomer  $\alpha$ . The enzymes responsible for the C-3-epimerization have not been identified to present date. It was also proposed by Reddy *et al.* that this pathway might be used for metabolites that resist inactivation through C-24 oxidation [18] a phenomenon well characterized in the bile acid metabolism where the reaction is catalyzed by bile acid hydroxysteroid dehydrogenase [27]. This pathway plays also a major role in the activation and/or inactivation of steroid hormones such as androgens [28].

Despite a lower binding affinity than calcitriol,  $1\alpha,25(\text{OH})_2\text{-}3\text{-epi-D}_3$  possess significant biological activity only in specific tissues where it is produced [29]. The transcriptional response of the  $1\alpha,25(\text{OH})_2\text{-}3\text{-epi-D}_3$  compound varies for different VDR-regulated genes in different tissues. For instance, it shows lower activation of osteocalcin gene and lower HL60 differentiation [30] but has almost equipotent activity to  $1\alpha,25(\text{OH})_2\text{D}_3$  in inhibiting cellular proliferation in keratinocytes [19] and in suppressing parathyroid secretion in bovine parathyroid cells [25]. These *in vitro* properties associated with its low calcemic activity [31,32] assign potential therapeutic interest to this compound.

To further unveil, the structural mechanism and structure-activity relationships of  $1\alpha,25(\text{OH})_2\text{-}3\text{-epi-D}_3$ /hVDR-LBD complex, we describe a more effective synthetic route to the synthesis of  $1\alpha,25(\text{OH})_2\text{-}3\text{-epi-D}_3$ , some of its *in vitro* biological properties and the crystal structure of its complex with hVDR LBD.

## Results and Discussion

### Synthesis of the $1\alpha,25(\text{OH})_2\text{-}3\text{-epi-D}_3$

The synthesis of the target  $1\alpha,25(\text{OH})_2\text{-}3\text{-epi-D}_3$  (**1**, Scheme S1) was first described by Okamura's group at Riverside from (*R*)-carvone using the diyne approach (13 steps, 8.5%) [33]. We describe here an efficient and alternative convergent synthesis of **1** from (*S*)-carvone (9 steps, 13%) that features a palladium catalyzed tandem process that produces the vitamin D triene unit stereoselectively in one pot by coupling enol triflate **3** (A-ring fragment) with an alkenyl metal intermediate **2** (CD-side chain fragment) [34]. For reproducibility reasons we employed Indium intermediates ( $\text{M} = \text{InR}_2$ ) instead of Zinc intermediates [35–37].

### Synthesis of the A-ring fragment **3**

Our synthesis starts with commercial (*S*)-carvone (**4**, Scheme S2), which was reduced under Luche conditions [38] to alcohol **5a** and its epimer **5b** (9:1 ratio as determined by  $^1\text{H-NMR}$ ). The mixture of alcohols **5** was subjected to Sharpless epoxidation [39] to provide the desired epoxyalcohol **6a** (58% yield, two steps) and the starting ketone **4** (28%). The formation of **4** can be explained by oxidation of **5a** through the corresponding chair-like equatorially oriented vanadium ester intermediate. *Tert*-butyldimethylsilyl protection of **6a** gave **6b** in 96% yield. Side-chain degradation on **6b** by Daniewski's method [40] afforded alcohol **7a** (71%), which was protected to **7b** in the usual way (91%). Epoxide **7b** was converted in 77% yield to dibromide **8b** by the two-step sequence: 1) oxidative cleavage with periodic acid; 2) Corey-Fuchs side-chain extension [41]. Finally, consecutive treatment of **8b** with lithium diisopropylamide and *n*-butyllithium followed by trapping of the resulting enolate with *N*-(5-*Cl*-2-pyridil)bis(triflate) gave the desired enol triflate **3** in 76% yield [42].

### Synthesis of the upper fragment **2** and

#### $1\alpha,25(\text{OH})_2\text{-}3\text{-epi-D}_3$ (**1b**)

Alkenyl bromide **10** was prepared from ketone **9** by a modified [43] Trost procedure [44]. Treatment of a mixture of bromide **10** and indium trichloride with *tert*-butyllithium, and coupling of the

resulting indium intermediate **2a** with enol triflate **3** in the presence of catalytic amounts of  $(\text{Ph}_3\text{P})_4\text{Pd}$  and  $(\text{dppf})\text{PdCl}_2$ , gave, after desilylation, the desired metabolite **1b** in 58% yield (Scheme S3). The detailed synthesis is described in the Methods S1.

### $1\alpha,25(\text{OH})_2\text{D}_3$ and $1\alpha,25(\text{OH})_2\text{-}3\text{-epi-D}_3$ show similar properties in coactivator peptide recruitment

The human transcriptional intermediary factor TIF2 coactivator (NCOA2) has been shown to interact with VDR [45]. The induced recruitment of TIF2 coactivator peptide bearing the 3rd LXXLL motif to the hVDR LBD was monitored in the presence of increasing concentrations of  $1\alpha,25(\text{OH})_2\text{D}_3$  or  $1\alpha,25(\text{OH})_2\text{-}3\text{-epi-D}_3$  using the luminescent oxygen channeling assays [46]. Our results show that  $\text{EC}_{50}$  value for both metabolites are in the lower nanomolar range, 1.2 and 2.5 nM for  $1\alpha,25(\text{OH})_2\text{D}_3$  and  $1\alpha,25(\text{OH})_2\text{-}3\text{-epi-D}_3$ , respectively (Figure 2A).

### $1\alpha,25(\text{OH})_2\text{D}_3$ and $1\alpha,25(\text{OH})_2\text{-}3\text{-epi-D}_3$ induce expression of vitamin D target genes in human breast cancer (MCF-7) cells with similar potency

The transactivation potency of  $1\alpha,25(\text{OH})_2\text{-}3\text{-epi-D}_3$  has been reported for several VDR target genes in different model cell lines such as MG-63 or ROS17/2.8 osteosarcoma cells [24,30]. While the transcriptional activity in MG-63 cells using a vitamin D-responsive element (VDRE) from human *osteocalcin* (−848/+10) and rat *CYP24* (−291/+9) gene promoters was lower upon stimulation with  $1\alpha,25(\text{OH})_2\text{-}3\text{-epi-D}_3$  compared to  $1\alpha,25(\text{OH})_2\text{D}_3$  [47], using 2xVDREs reporter from *CYP24* gene promoter in human melanoma G-361 cells comparable transcriptional activity was observed [48]. This response is mainly achieved in cells in which the  $1\alpha,25(\text{OH})_2\text{-}3\text{-epi-D}_3$  metabolite is produced [29]. We monitored the dose-dependent VDR induced transcriptional activity in human breast cancer cells (MCF-7) cells transfected with human *CYP24* promoter (−414 to −64) containing VDRE fused to reporter *luciferase* gene (Figure 2B). Here, we show that  $1\alpha,25(\text{OH})_2\text{-}3\text{-epi-D}_3$  is slightly less potent than  $1\alpha,25(\text{OH})_2\text{D}_3$  in directing transactivation assay as the  $\text{EC}_{50}$  induced by  $1\alpha,25(\text{OH})_2\text{-}3\text{-epi-D}_3$  is twice higher than that of  $1\alpha,25(\text{OH})_2\text{D}_3$  (5.9 nM vs 2.9 nM). This difference is in agreement with our results obtained from cell free coactivator peptide recruitment assays. Our transactivation assays show that the dose-dependent comparison between the  $1\alpha,25(\text{OH})_2\text{-}3\text{-epi-D}_3$  and  $1\alpha,25(\text{OH})_2\text{D}_3$  reveals that at 50% of the dose-response, the transcriptional activity of the 3-epimer is 65% of that obtained with  $1\alpha,25(\text{OH})_2\text{D}_3$ . Statistical analysis revealed a significant correlation between both the induced-coactivator recruitment and transactivation assays (Pearson  $r = 0.961^{**}$  and  $r = 0.986^{**}$ , respectively), indicating the similarity in the course of the dose response curves for both  $1\alpha,25(\text{OH})_2\text{D}_3$  and  $1\alpha,25(\text{OH})_2\text{-}3\text{-epi-D}_3$ . The reason for the discrepancy from the previously reported lower transactivation potential of  $1\alpha,25(\text{OH})_2\text{-}3\text{-epi-D}_3$  may have its origin in different *CYP24* promoter fragment used in our experiments. Although, the EMSA assays with nuclear extracts and *in vitro* translated full length VDR and RXR reported by Nakagawa *et al.* [47] showed decreased DNA complex formation of VDR-RXR heterodimer in the presence of  $1\alpha,25(\text{OH})_2\text{-}3\text{-epi-D}_3$  compared to  $1\alpha,25(\text{OH})_2\text{D}_3$ , the same authors showed using two-hybrid system that the strength of VDR-RXR heterodimerization in presence of 10nM of the 3-epimer is 40% compared to that observed for  $1\alpha,25(\text{OH})_2\text{D}_3$ .

### Cell specific effects of $1\alpha,25(\text{OH})_2\text{-}3\text{-epi-D}_3$

The magnitude of  $1\alpha,25(\text{OH})_2\text{-}3\text{-epi-D}_3$ -mediated specific biological outcomes versus that induced by  $1\alpha,25(\text{OH})_2\text{D}_3$  is cell line specific. As such, it is established based only on CD11b

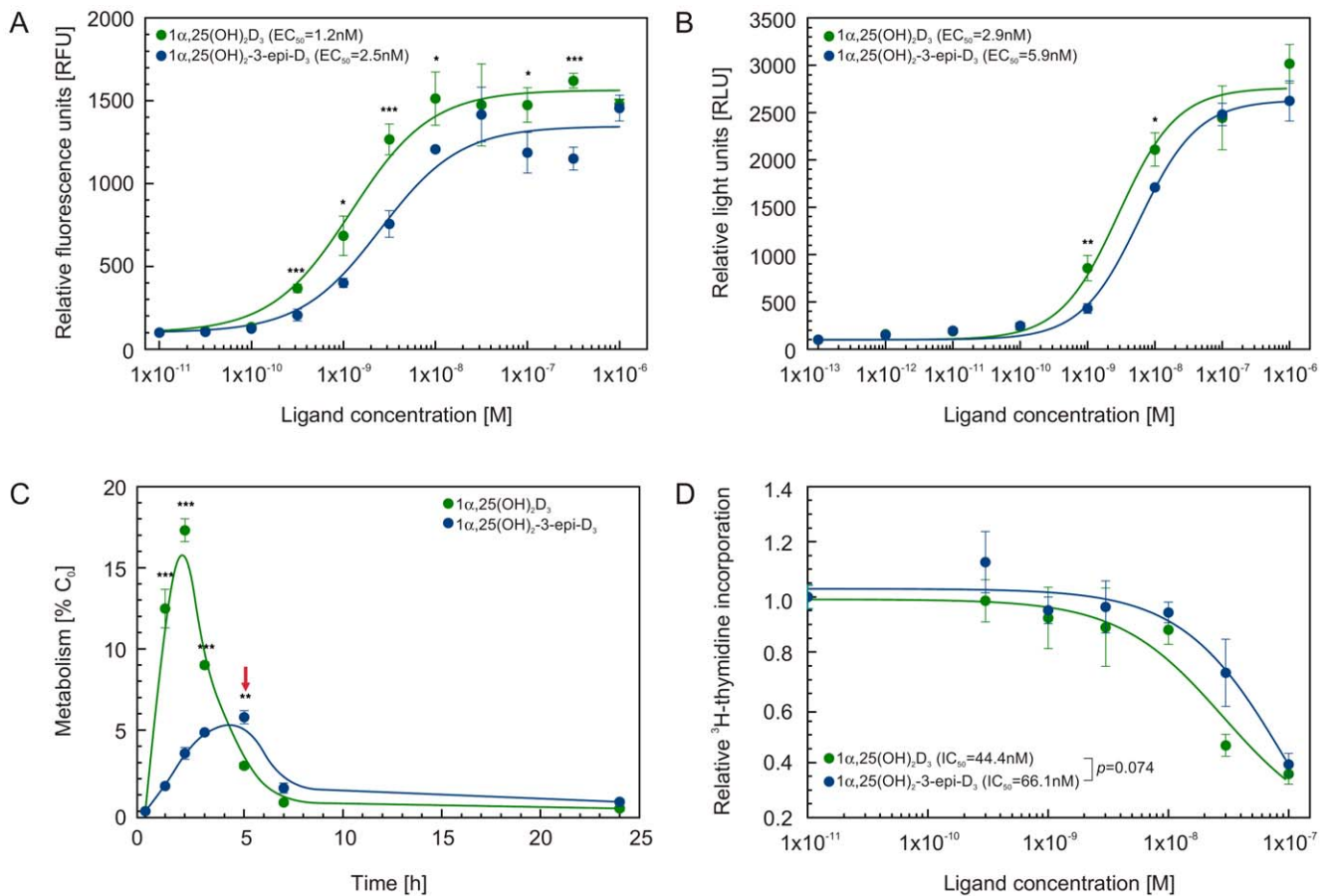


**Figure 2.  $1\alpha,25(\text{OH})_2\text{D}_3$  and  $1\alpha,25(\text{OH})_2\text{-}3\text{-epi-D}_3$  show similar biological properties.** (A) Coactivator peptide recruitment assay was performed using AlphaScreen method in the presence of increasing concentrations of either  $1\alpha,25(\text{OH})_2\text{D}_3$  (green circles) or  $1\alpha,25(\text{OH})_2\text{-}3\text{-epi-D}_3$  (blue circles). The data represents two independent measurements in triplicates for which the mean and the S.D. of the mean was calculated. (B) Transactivation assays were performed in human breast cancer cells MCF7 cells with subsequent treatments of the increasing concentrations of either  $1\alpha,25(\text{OH})_2\text{D}_3$  (green circles) or  $1\alpha,25(\text{OH})_2\text{-}3\text{-epi-D}_3$  (blue circles). For every triplicate the mean and the S.D. were calculated. (C) Metabolism of  $^3\text{H}$ - $25(\text{OH})\text{D}_3$  in human keratinocytes. Kinetics of the primary metabolite  $1\alpha,25(\text{OH})_2\text{D}_3$  and its 3-epimer, is shown. The time point 5 h, where the  $1\alpha,25(\text{OH})_2\text{-}3\text{-epi-D}_3$  is the major metabolite is highlighted with red arrow. Confluent keratinocytes derived from lid skin were incubated in KGM (0.06 mM calcium) with 20.6 nM  $^3\text{H}$ [26,27]- $25(\text{OH})\text{D}_3$  for the indicated time periods.  $\text{CHCl}_3$ -extracts of the incubations were analyzed on Zorbax-Sil and individual metabolites identified by matching with authentic reference compounds and quantified as described in Materials and Methods. Data ( $\pm$  SD) was calculated from duplicate experiment. (D) Anti-proliferative cellular effect of  $1\alpha,25(\text{OH})_2\text{D}_3$  and  $1\alpha,25(\text{OH})_2\text{-}3\text{-epi-D}_3$  in human keratinocytes. Keratinocytes in serum-free KGM (0.06 mM calcium) were seeded into 96-well plates and 24 h later the indicated metabolites (range 0.1–100 nM). After further 24 h, 1  $\mu\text{Ci}$   $^3\text{H}$ -thymidine was applied to each well and its incorporation determined as described in Methods. Data are mean values ( $\pm$  SD) from a representative experiment out of two independent studies, each done in triplicates. For all experiments Student's unpaired t-test was performed and  $p$ -values were calculated between values obtained for  $1\alpha,25(\text{OH})_2\text{D}_3$  and  $1\alpha,25(\text{OH})_2\text{-}3\text{-epi-D}_3$  (\*  $p < 0.05$ , \*\*  $p < 0.01$ , \*\*\*  $p < 0.001$ ).

doi:10.1371/journal.pone.0018124.g002

antigen positive cell numbers that  $1\alpha,25(\text{OH})_2\text{-}3\text{-epi-D}_3$  is biologically less potent than  $1\alpha,25(\text{OH})_2\text{D}_3$  in the human leukemia anti-proliferation and pro-differentiation cellular model (HL60), compared to  $1\alpha,25(\text{OH})_2\text{D}_3$  [47]. We monitor the precise dose-dependent study of  $1\alpha,25(\text{OH})_2\text{-}3\text{-epi-D}_3$  - directed HL60 cell anti-proliferation and differentiation by live cell enumeration and flow cytometry based on the expression of both CD11c and CD14 cell surface markers. In our experiments for both,  $1\alpha,25(\text{OH})_2\text{D}_3$  and  $1\alpha,25(\text{OH})_2\text{-}3\text{-epi-D}_3$ , only the saturating 100 nM concentration of ligand reduced the numbers of HL60 cells (Figure S1 and Methods S2). Although for  $1\alpha,25(\text{OH})_2\text{-}3\text{-epi-D}_3$  the related percentage of single positive or double CD11c/CD14 sub-populations was higher compared to that observed in control incubations, it was markedly reduced compared to that induced with 100 nM  $1\alpha,25(\text{OH})_2\text{D}_3$ , consistent with the previous study [47].

Further, we hypothesized about the absence of the  $1\alpha,25(\text{OH})_2\text{-}3\text{-epi-D}_3$  signaling in HL60 cellular model and thus turned to characterize some of the biological properties of  $1\alpha,25(\text{OH})_2\text{-}3\text{-epi-D}_3$  in cells where it is produced [20,21]. We first determined the kinetics of *CYP27B1*- and *CYP24A1*-catalyzed oxidation by monitoring the major lipophilic metabolites arising from a single pulse of  $^3\text{H}$ [26,27]- $25(\text{OH})\text{D}_3$  at physiological concentration (20.6 nM). During the first two hours, we observed a rapid appearance of  $1\alpha,25(\text{OH})_2\text{D}_3$ , from which at a slower rate the 3-epimer was irreversibly formed. In total, some 60 independent incubation experiments were performed on the kinetics of  $^3\text{H}$ [26,27]- $25(\text{OH})\text{D}_3$  using primary keratinocytes from various donors and skin sites. In all experiments, highly comparable time course of  $1\alpha,25(\text{OH})_2\text{D}_3$  and  $1\alpha,25(\text{OH})_2\text{-}3\text{-epi-D}_3$  were recorded with 3-epimer exceeding  $1\alpha,25(\text{OH})_2\text{D}_3$  after longer incubation as shown in Figure 2C and in the detailed HPLC analysis in Figure

S2 and Methods S2. Since the  $1\alpha,25(\text{OH})_2\text{-}3\text{-epi-D}_3$  is present steadily up to 5 h in rather high concentration in this tissue and the fact that the primary genomic effects of hVDR ligands are exerted in first hours suggested that primary keratinocytes may be a good cellular model to investigate the anti-proliferative actions of this metabolite. Therefore we determined the dose-dependent anti-proliferative effects of  $1\alpha,25(\text{OH})_2\text{D}_3$  and  $1\alpha,25(\text{OH})_2\text{-}3\text{-epi-D}_3$  using  $^3\text{H}$ -thymidine incorporation assay (Figure 2D), and found that the  $\text{IC}_{50}$  values for  $1\alpha,25(\text{OH})_2\text{D}_3$  and  $1\alpha,25(\text{OH})_2\text{-}3\text{-epi-D}_3$  were highly similar (41.4 and 66.1 nM, respectively) with no significant statistical difference (using unpaired *t*-test  $p = 0.074$ ). In addition, we correlated the course of the anti-proliferation data between the two epimers and find a strong correlation (Pearson  $r = 0.940^{**}$ ) between them indicating the similar anti-proliferative activity for  $1\alpha,25(\text{OH})_2\text{D}_3$  and  $1\alpha,25(\text{OH})_2\text{-}3\text{-epi-D}_3$ . The anti-proliferative effects of the two metabolites are comparable and they are in close agreement with our coactivator peptide recruitment (Figure 2A) and reporter gene assays (Figure 2B). Although in this assay we cannot totally exclude the possibility that the potential cell type specific difference in the function of the two natural ligands may be partly due to the accumulation of  $1\alpha,25(\text{OH})_2\text{-}3\text{-epi-D}_3$  in  $1\alpha,25(\text{OH})_2\text{D}_3$  treated cells with C3-epimerization ability leading to additive effect, we consider this accumulation process as a naturally occurring *in vivo* physiological event when  $1\alpha,25(\text{OH})_2\text{D}_3$  is present in these cells.

#### Overall structure of the hVDR complexed to $1\alpha,25(\text{OH})_2\text{-}3\text{-epi-D}_3$

The mechanistic action of analogues of  $1\alpha,25(\text{OH})_2\text{D}_3$  is unveiled by the determination at high resolution of the crystal structure of their complexes with the VDR LBD [49–53]. We solved the crystal structure of the complex formed by  $1\alpha,25(\text{OH})_2\text{-}3\text{-epi-D}_3$  with the hVDR LBD mutant previously used to solve the structures of hVDR LBD in complexes with  $1\alpha,25(\text{OH})_2\text{D}_3$  or several synthetic agonists [49–54]. The crystal was isomorphous and the structure of hVDR LBD bound to  $1\alpha,25(\text{OH})_2\text{-}3\text{-epi-D}_3$

determined at a resolution of 1.9 Å (PDB ID: 3A78). The crystallographic data are summarized in Table S1. After refinement of the protein alone, the map showed an unambiguous electron density where to fit the ligand (Figure 3B). The complex formed by the hVDR LBD bound to  $1\alpha,25(\text{OH})_2\text{-}3\text{-epi-D}_3$  adopts the canonical active conformation as described in all previously reported agonist-bound nuclear receptor LBDs (Figure 3A). The conformation of the activation helix 12 is strictly maintained. When compared to the structure of hVDR LBD- $1\alpha,25(\text{OH})_2\text{D}_3$  complex, the atomic coordinates of hVDR LBD bound to  $1\alpha,25(\text{OH})_2\text{-}3\text{-epi-D}_3$  show very small root-mean-square deviation (RMSD) of 0.17 Å for all 255 C $\alpha$  atoms, reflecting its high structural homology.

#### Conformation of the $3\alpha$ -epimer in the ligand-binding pocket of hVDR

The  $1\alpha,25(\text{OH})_2\text{-}3\text{-epi-D}_3$  is buried in the predominantly hydrophobic ligand-binding pocket (LBP) of the VDR. The conformation of the 3-epi-hydroxyl group does not modify the A-ring chair conformation of the ligand. Furthermore the seco B-, C-, D-rings, and the aliphatic side chain present conformations similar to those observed with  $1\alpha,25(\text{OH})_2\text{D}_3$  (Figure 3B and C).

In the complexes of hVDR LBD bound to  $1\alpha,25(\text{OH})_2\text{D}_3$  versus  $1\alpha,25(\text{OH})_2\text{-}3\text{-epi-D}_3$ , the distance between the C1-OH and the C25-OH groups varies from 13.1 Å to 12.7 Å and between the C3-OH and the C25-OH groups from 15.3 Å to 16.0 Å, respectively. The adaptation of the hVDR's LBP to different ligands can be described with the differential changes in the volumes of LBPs and bound ligands. In addition the parameter representing the % of LBP filling with ligand can provide useful information about the activity of ligand [55]. All these parameters are summarized in Table 1. Although the two diastereomer have the same molecular weight and differ only in the position of the C3-OH group, the  $1\alpha,25(\text{OH})_2\text{-}3\text{-epi-D}_3$  takes a slightly more compact conformation in the LBP. The graphical 0.2 Å mesh representation of the superimposed LBPs presented in Figure 4A

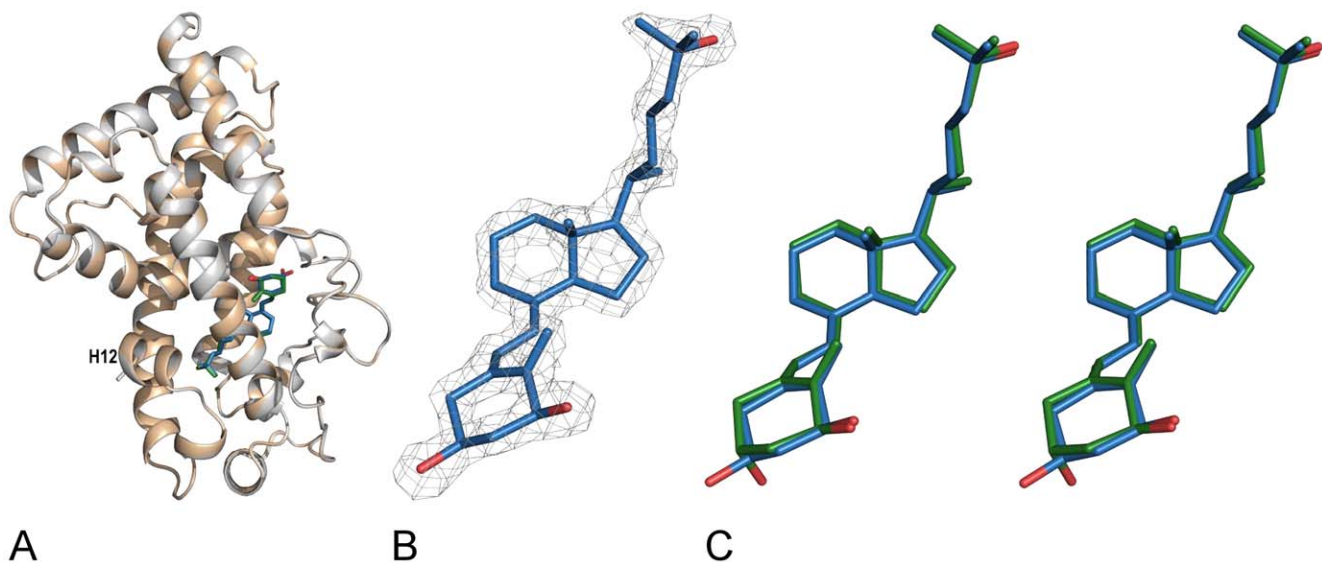


**Figure 3. Overall structure of the VDR- $1\alpha,25(\text{OH})_2\text{-}3\text{-epi-D}_3$  and conformation of the bound ligand.** (A) Superimposition of the hVDR LBD-  $1\alpha,25(\text{OH})_2\text{-}3\text{-epi-D}_3$  (blue) and the hVDR LBD- $1\alpha,25(\text{OH})_2\text{D}_3$  (white). The ligands are shown in stick representation in blue for the  $1\alpha,25(\text{OH})_2\text{-}3\text{-epi-D}_3$  and in green for the  $1\alpha,25(\text{OH})_2\text{D}_3$ . (B) The  $1\alpha,25(\text{OH})_2\text{-}3\text{-epi-D}_3$  is shown in its  $F_o - F_c$  electron density omit map contoured at 3  $\sigma$ . The ligand is shown in stick representation with carbon and oxygen atoms in blue and red, respectively. (C) Stereo view of the ligand 3D conformations of  $1\alpha,25(\text{OH})_2\text{-}3\text{-epi-D}_3$  (blue) and  $1\alpha,25(\text{OH})_2\text{D}_3$  (green) in their VDR ligand-binding pockets (LBP). doi:10.1371/journal.pone.0018124.g003

**Table 1.** Volume of VDR ligands and their resulting LBPs.

Ligand	Ligand volume [ $\text{\AA}^3$ ] *	Ligand volume [%]*	LBP volume [ $\text{\AA}^3$ ]**	LBP volume [%]**	Filling of the LBP with ligand [%]
$1\alpha,25(\text{OH})_2\text{D}_3$	416.56	100.00	667.13	100.00	62.44
$1\alpha,25(\text{OH})_2\text{-}3\text{-epi-D}_3$	407.65	97.86	633.75	95.00	64.32

The absolute values in  $\text{\AA}^3$  as well as relative values in reference to those of  $1\alpha,25(\text{OH})_2\text{D}_3$  (100%) are indicated. From these values the percent filling of the LBP with ligands was also calculated.

\*and \*\* Connolly solvent accessible surfaces calculated by GRASP and Voidoo respectively The quality of the cubic grid spacing for the surface for both ligands and LBP = 0.5  $\text{\AA}$ .

doi:10.1371/journal.pone.0018124.t001

and B show the surface area which is enlarged in case of  $1\alpha,25(\text{OH})_2\text{D}_3$  (in green) and the one enlarged in case of  $1\alpha,25(\text{OH})_2\text{-}3\text{-epi-D}_3$  bound hVDR LBP (in blue). This suggests that the hydrophobic residues lining the LBP are closer to the 3-epimer and may compensate for the canonical hydrogen bonds. We observed a notable adaptation with the displacement of the side chain of the residue Tyr147 by 2.0  $\text{\AA}$  compared to the  $1\alpha,25(\text{OH})_2\text{D}_3$  bound complex and the reorientation of the Glu277 side chain away from the  $1\alpha,25(\text{OH})_2\text{-}3\text{-epi-D}_3$  due to the  $\alpha$ -position of the C3-OH group (Figure 4B). These specific rearrangements lead to a more compact conformation resulting in a 5% decrease in the volume of the LBP compared to  $1\alpha,25(\text{OH})_2\text{D}_3$ .

#### Specific interactions of the $1\alpha,25(\text{OH})_2\text{-}3\text{-epi-D}_3$

The hydrophobic and electrostatic interactions between the receptor and the ligand are similar between the two structures except around the C3-OH group. While the C1-OH and C25-OH display the canonical hydrogen bonds, the 3-epi-OH of  $1\alpha,25(\text{OH})_2\text{-}3\text{-epi-D}_3$  interacts through hydrogen bonding only with Tyr143 instead of interacting with both Tyr143 and Ser278 (Figure 5). A significant feature of the  $1\alpha,25(\text{OH})_2\text{-}3\text{-epi-D}_3$  is the

compensation of the loss of interaction with Ser278 by a water-mediated hydrogen bond with the water molecule  $\text{H}_2\text{O}1$  (W1 in [50]). As such, the position of water  $\text{H}_2\text{O}1$  is moved 0.7  $\text{\AA}$  towards  $1\alpha,25(\text{OH})_2\text{-}3\text{-epi-D}_3$ , thereby facilitating the specific water-mediated contacts. This water molecule is part of the network connecting another water molecule  $\text{H}_2\text{O}2$  to Arg274. All these water molecules are also present in the  $1\alpha,25(\text{OH})_2\text{D}_3$ -hVDR complex [50]. The C3-OH hydrogen bonds have longer distances in the 3-epimer (3.0  $\text{\AA}$  instead of 2.8  $\text{\AA}$  with Tyr143 and 3.1  $\text{\AA}$  with the water molecule instead of 2.9  $\text{\AA}$  with Ser278). A study on the mutations of the residues forming the hydrogen bonds with the hydroxyl groups of  $1\alpha,25(\text{OH})_2\text{-}3\text{-epi-D}_3$  revealed that mutated residues contacting the 3-hydroxyl group are the less affected in term of activity. Mutation of Ser278 in Ala may result in a lower binding affinity for  $1\alpha,25(\text{OH})_2\text{D}_3$  [56] while showing a similar potency to activate the transcription [57,56]. Due to the shift of the side chain of Tyr147, a hydrophobic interaction with this residue is lost in the 3-epimer structure. These structural data agree well with the lower binding affinity of this compound for VDR and to its induced biological activity.

In conclusion, we described a more effective synthesis of the highly stable  $1\alpha,25(\text{OH})_2\text{-}3\text{-epi-D}_3$ , a natural metabolite. We have

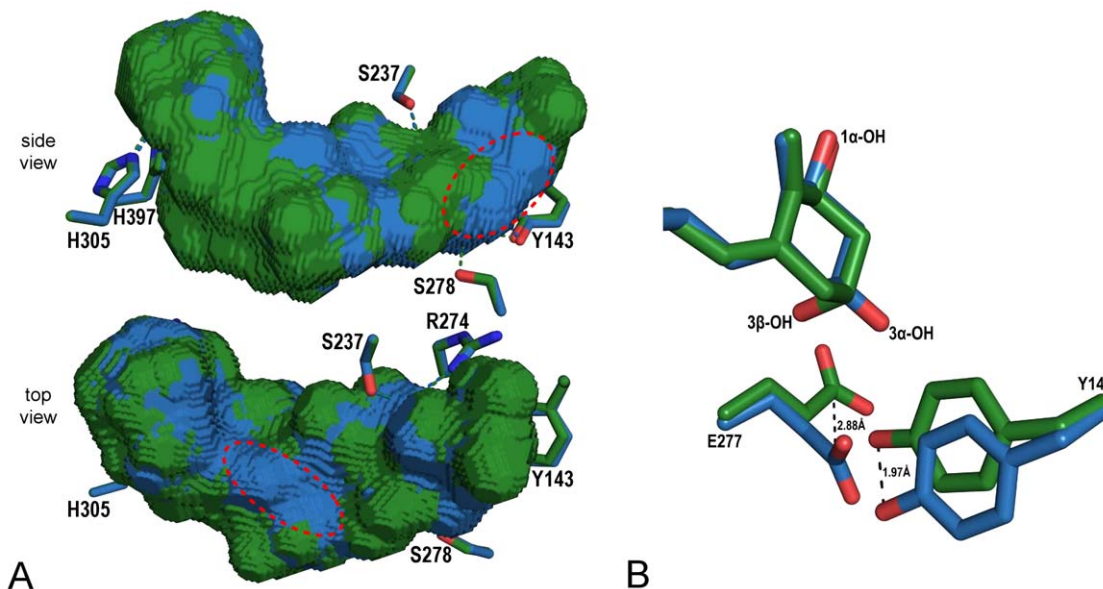


**Figure 4. Adaptability of the hVDR LBP upon  $1\alpha,25(\text{OH})_2\text{-}3\text{-epi-D}_3$  binding.** (A) The adaptation of the LBP is depicted by mesh representation of the superimposed LBP volumes calculated with Voidoo software. The green surface represent the LBP area where the  $1\alpha,25(\text{OH})_2\text{D}_3$  bound pocket is larger. The blue area represents similar increase but for  $1\alpha,25(\text{OH})_2\text{-}3\text{-epi-D}_3$  and the two main expanded regions are highlighted with red circles. (B) Adaptation of the residues Tyr147 and Glu277 in the LBP of the  $1\alpha,25(\text{OH})_2\text{-}3\text{-epi-D}_3$  hVDR complex. The distances between the ligand-specific positions of the residues are displayed in  $\text{\AA}$ .  
doi:10.1371/journal.pone.0018124.g004

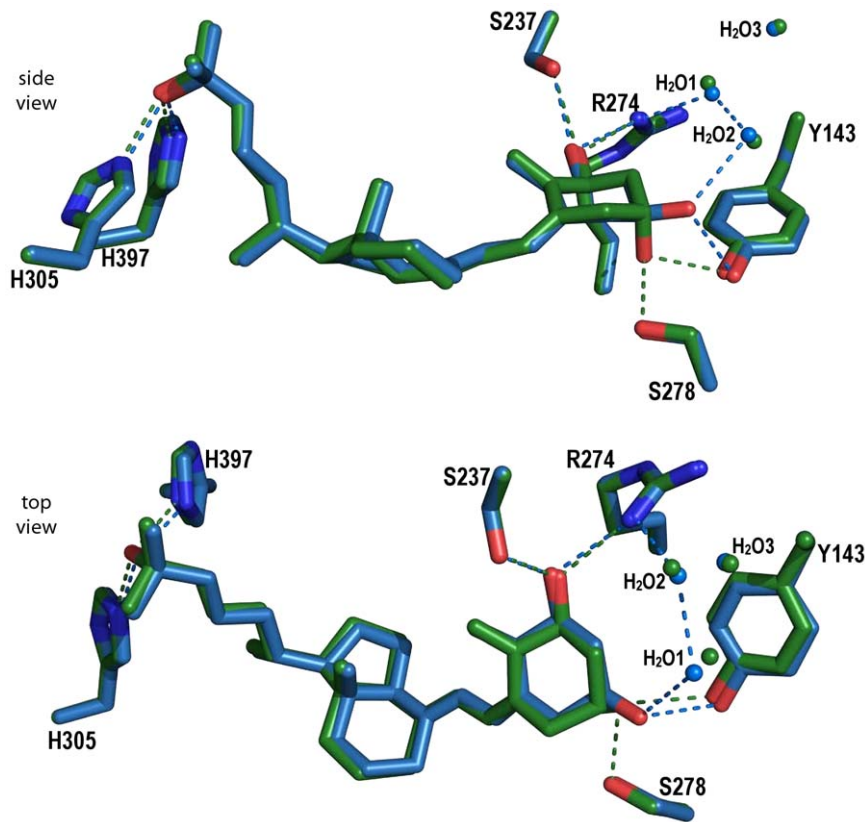


**Figure 5. Specific interactions of  $1\alpha,25(\text{OH})_2\text{-}3\text{-epi-D}_3$  in the LBP of the hVDR.** The ligands and residues in the superimposed structures are highlighted in color ( $1\alpha,25(\text{OH})_2\text{-}3\text{-epi-D}_3$  in blue and in  $1\alpha,25(\text{OH})_2\text{D}_3$  green) and the important water molecules are represented with colored dots. doi:10.1371/journal.pone.0018124.g005

solved the crystal structure of hVDR LBD in complex with  $1\alpha,25(\text{OH})_2\text{-}3\text{-epi-D}_3$ , which provides a mechanistic insight for the specific recognition of the two naturally occurring 3-epimers by hVDR. Indeed, the crystal structure reveals that the 3-epimer metabolite maintains the number of H-bonds by an alternative water-mediated interaction. In MCF-7 cells, the  $1\alpha,25(\text{OH})_2\text{-}3\text{-epi-D}_3$  on *CYP24* gene promoter retains significant transcriptional activity. In addition, the anti-proliferative action of  $1\alpha,25(\text{OH})_2\text{-}3\text{-epi-D}_3$  is cell specific and the  $\text{IC}_{50}$  values of  $1\alpha,25(\text{OH})_2\text{D}_3$  and  $1\alpha,25(\text{OH})_2\text{-}3\text{-epi-D}_3$  in primary keratinocytes are in the same nanomolar range. Therefore, we conclude that the C3-epimerization pathway produces an active metabolite with similar biochemical and biological properties to those of the  $1\alpha,25(\text{OH})_2\text{D}_3$ . The physiological role of this pathway as the specific biological action of the 3-epimer remains unclear and needs further investigation. However, its high metabolic stability together with its significant biologic activity makes this natural metabolite an interesting ligand for clinical applications. Further study on its target specificity and selectivity is required to the design of selective analogues. Our new findings contribute to a better understanding at molecular level how natural metabolites of  $1\alpha,25(\text{OH})_2\text{D}_3$  lead to significant activity in biological systems.

## Materials and Methods

### Ligands

$1\alpha,25(\text{OH})_2\text{D}_3$  was purchased from Cayman Chemical (Tallinn, Estonia) and the synthesis of  $1\alpha,25(\text{OH})_2\text{-}3\text{-epi-D}_3$  is described in more details in the Methods S1. Additional ligands and reference compounds are described in Methods S2. IUPAC rules were used

for the name of the compounds. In addition to NMR spectra (summarized in Methods S1), HPLC analysis was used to determine the purity (>95%) of the vitamin D analogues.

### Protein expression vectors for transactivation assays

Full-length cDNAs for human VDR [58] was subcloned into the T7/SV40 promoter-driven pSG5 expression vector (Stratagene, Heidelberg, Germany) and full-length cDNAs for green fluorescent protein (GFP) [59] was subcloned into parent vector resulting the pEGFP-C2 mammalian expression vector (Clontech Laboratories, Inc., USA).

### Luciferase reporter gene construct

The fragment of the proximal promoter region (−414 to −64) of the human *CYP24A1* gene was fused with the *thymidine kinase* promoter driving the firefly *luciferase* reporter gene [60].

### Coactivator peptide recruitment assays

Biochemical interaction between human VDR-LBD and the coactivator peptide in the presence of  $1\alpha,25(\text{OH})_2\text{D}_3$  or  $1\alpha,25(\text{OH})_2\text{-}3\text{-epi-D}_3$  was assayed using the AlphaScreen technology. The assay was performed in white opaque 384-well microplate (OptiPlate-384 Perkin Elmer) using a final volume of 15  $\mu\text{l}$  containing final concentrations of 100 nM *E. coli*-expressed hexahistidine (6xHis)-tagged VDR-LBD protein, 20 nM of the human TIF2-3 biotinylated peptide (Btm-QEPVSPKKKENALL-RYLLDKDDTKD), and 10  $\mu\text{g}/\text{ml}$  of both AlphaLISA  $\text{Ni}^{2+}$ -chelate acceptor beads and (AL108C) and AlphaScreen streptavidin coated donor beads (6760002S) in an assay buffer containing

50 mM MOPS pH=7.4, 50 mM NaF, 50 mM CHAPS, and 100  $\mu\text{g/ml}$  bovine serum albumin. Different concentrations of  $1\alpha,25(\text{OH})_2\text{D}_3$  or  $1\alpha,25(\text{OH})_2\text{-}3\text{-epi-D}_3$  dissolved in DMSO (maintained at a final concentration of 1%) were added as indicated. The experiment represents two independent measurements in triplicates for, which the mean and the S.D. of the mean was calculated.

### Transient transfections and luciferase reporter gene assays

MCF-7 cells were seeded into 24-well plates (100,000 cells/well) and grown overnight in phenol red-free Dulbecco's modified Eagle's medium (DMEM) supplemented with 10% charcoal-stripped fetal bovine serum (FCS) and 0.6  $\mu\text{g/ml}$  insulin. Plasmid DNA containing liposomes were formed by incubating 40 ng of an expression vector for hVDR, 100 ng of reporter plasmid and 10 ng pEGF-C2 with Fugene 6 (Roche Diagnostics, Switzerland) transfection reagent according to the recommendation of the manufacturer for 15 min at room temperature. After dilution with 500  $\mu\text{l}$  of phenol red-free DMEM, the liposomes were added to the cells. Phenol red-free DMEM supplemented with 500  $\mu\text{l}$  of 20% charcoal-stripped FCS was added 4 h after transfection, in the presence of ligands or solvent. The cells were lysed 16 h after the onset of stimulation using reporter gene lysis buffer (Roche Diagnostics, Switzerland). The lysates were assayed for luciferase activity as recommended by the supplier (Perkin-Elmer, The Netherlands). The luciferase activities were normalized to GFP expression. Data represent one triplicate for which the mean and the S.D. of the mean was calculated.

### Data analysis for dose response curves

A non-linear curve fit was performed for the AlphaScreen and reporter gene assay experimental dose response data and from sigmoidal dose response curve then the  $\text{EC}_{50}$  values for the respective ligands were calculated using GraphPad Prism 4 (GraphPad Software Inc., San Diego, CA). The Student's unpaired *t*-test and Pearson correlation were performed with the SPSS software (SPSS Inc., version 14.0, Chicago, IL, USA).

### Keratinocyte cell cultures

Normal human keratinocytes were isolated from fresh adult skin obtained from surgery and immediately transported to the laboratory under sterile conditions. Isolation and culture under serum-free conditions and without a feeder layer followed a modified protocol as used by Bikle *et al* [11]. The isolated epidermis was incubated in a 0.25% trypsin solution for 45 min at 37°C. Thereafter, the cells were scraped off and put in 50 ml Hank's balanced salt solution (HBSS) containing 10% FCS to block further trypsin digestion and centrifuged at 2000 rpm/2 min. The resulting cell pellet was suspended in Keratinocyte Growth Medium (KGM, Clonetics Corp., San Diego), a defined serum-free medium at low (0.06 mM) calcium containing 0.1 ng/ml epidermal growth factor, 5  $\mu\text{g/ml}$  insulin, 0.5  $\mu\text{g/ml}$  hydrocortisone, bovine pituitary extract, antibiotics (gentamycin, amphotericin) gave the primary culture. After 24 h, the cells were incubated at 37°C in 95% air/5%  $\text{CO}_2$  and the attached cells were washed and provided with fresh KGM medium. The culture medium was changed every other day and the cells were passaged when they reached 80–90% confluency (usually 6–10 days after plating).

### Incubations of primary keratinocytes with $^3\text{H-}25(\text{OH})\text{D}_3$

Confluent human keratinocytes in 1 ml KGM and in 6-well plates were incubated in triplicates at 37°C with 20.6 nM  $^3\text{H-}$

$25(\text{OH})\text{D}_3$  (around 600 000 dpm/ml) for 1–23 h. Incubations were stopped with 1 ml methanol/well, the cells were scraped off, transferred to a test tube together with the supernatant and two washings (with 1 ml methanol and 0.8 ml water). Unmodified  $^3\text{H-}25(\text{OH})\text{D}_3$  and most of the products were totally extracted from the combined solutions plus cell pellet according to the method of Bligh and Dyer [61] by three subsequent extractions with 2, 1 and 1 ml volumes of  $\text{CHCl}_3$  at room temperature.  $^3\text{H-}$ activity in the  $\text{CHCl}_3$ -phase, in the water and total  $^3\text{H-}$ yield were determined. The combined  $\text{CHCl}_3$  extracts were then evaporated under argon at 35°C, the residues dissolved in 0.4 ml ethanol and an aliquot (containing around 250 000 dpm  $^3\text{H-}$ activity) subjected to HPLC-analysis (see Methods S2).

### $^3\text{H-}$ Thymidine incorporation (anti-proliferation assay in primary keratinocytes)

Keratinocytes (second passage) in 200  $\mu\text{l}$  KGM (low calcium) were plated in 96-well plates at an initial density of  $10^4$  cells/well, kept 24 h at 37°C in an incubator with 95% air/5%  $\text{CO}_2$ . Thereafter, the test compounds  $1,25(\text{OH})_2\text{D}_3$  or its 3-epimer were added in 1  $\mu\text{l}$  ethanol to give final concentrations ranging from 0 to 100 nM, each condition in triplicates. After further 24 h, 50  $\mu\text{l}$   $^3\text{H-}$ thymidine (1  $\mu\text{Ci}$ ) were added and incubation continued for additional 7 h. Then, incubations were stopped by cell harvesting (Filtermate 196 Harvester, Packard-Canberra) and lysis: After removing the supernatant (see below), the adherent cells were released by 5 min treatment with 100  $\mu\text{l}$  0.125% trypsin in PBS at 37°C, harvested on a filterplate and washed 3 x with redistilled water. After drying the plates, their bottoms were sealed with a film and 50  $\mu\text{l}$  scintillation cocktail (MicroScint O, Packard) were added. The whole plates were sealed with Packard Cover Film and  $^3\text{H-}$ activity counted on a Microplate Scintillation Counter (TopCount, Packard Canberra). To check whether proliferative ( $^3\text{H-}$ thymidine incorporating) cells could have been shed off, the supernatants were soaked through a 96-well filterplate (Unifilter Plate GF/C) and 3 x washed with redistilled water: in all conditions,  $^3\text{H-}$ activity was undetectable on these filterplates (in order to roughly assess cell numbers and check for substance related morphological changes/toxic effects, photographs were taken prior to compound addition and immediately before harvesting.) Data - used as means  $\pm$  SD - were normalized (incorporated  $^3\text{H-}$ activity sample vs. blank) and analyzed using the GRAFIT Erithacus 4.0.19 IC<sub>50</sub> software.

### Protein purification and Crystallization

Purification and crystallization of the hVDR LBD complexed with  $1\alpha,25(\text{OH})_2\text{-}3\text{-epi-D}_3$  were performed as previously described [49]. The LBD of the hVDR (residues 118-427  $\Delta$ 166-216) was cloned in pET-28b expression vector (Novagen) to obtain an N-terminal 6xHis fusion protein and was overproduced in *E. coli* BL21 (DE3) strain. Cells were grown in Luria Bertani medium and subsequently incubated for 6 h at 20°C with 1 mM isopropyl thio- $\beta$ -D-galactoside. The protein purification included a metal affinity chromatography step on a  $\text{Co}^{2+}$ -chelating resin (Clontech). The 6xHis tag was removed by thrombin digestion overnight at 4°C, and the protein was further purified by gel filtration on a Superdex S200 16/60. The sample buffer prior to protein concentration contained 10 mM Tris, pH=7.5, 100 mM NaCl, and 10 mM dithiothreitol. The protein was concentrated to 3.5 mg/ml and incubated in the presence of a 1.5-fold molar excess of ligand. The purity and homogeneity of the protein were assessed by SDS-PAGE. The protein crystals were obtained at 4°C by vapor diffusion method using crystals of hVDR LBD- $1\alpha,25(\text{OH})_2\text{D}_3$  as

microseeds. The reservoir solution contained 0.1 M MES and 1.4 M ammonium sulfate pH = 6.0.

### X-Ray data collection and structure determination

The crystal was mounted in fiber loop and flash cooled in liquid nitrogen after cryoprotection with a solution containing the reservoir plus 30% glycerol and 2% polyethylene glycol 400. Data collection from a single frozen crystal was performed at 100 K on the beamline ID29 of the European Synchrotron Radiation Facility (Grenoble, France). The crystal belongs to the orthorhombic space group  $P2_12_12_1$  with one monomer per asymmetric unit. Data were integrated and scaled using MOSFLM [62] (see statistics in Table S1). A rigid body refinement was used with the structure of the hVDR LBD complexed to  $1\alpha,25(\text{OH})_2\text{D}_3$  as a starting model. Refinement involved iterative cycles of manual building and refinement calculations. The programs Refmac [63] and COOT [64] were used throughout structure determination and refinement. The omit map from the refined atomic model of hVDR LBD was used to fit the ligand to its electron density, shown in Figure 2A. Individual B-atomic factors were refined isotropically. Solvent molecules were then placed according to unassigned peaks in the difference Fourier map. In the hVDR/ $1\alpha,25(\text{OH})_2\text{-}3\text{-epi-D}_3$  complex, refined at 1.9 Å with no  $\sigma$  cutoff, the final model consists of residues 118–423 ( $\Delta$ 166–216), the ligand, two sulphate ions and 372 water molecules. According to PROCHECK [65] 92.6% of peptide lies in most favored regions and 7.4% in additional allowed regions. Data are summarized in Table S1. The volumes of the ligand-binding pockets and ligands were calculated as previously reported [49].

### Supporting Information

**Figure S1 Biological properties of  $1\alpha,25(\text{OH})_2\text{D}_3$  and  $1\alpha,25(\text{OH})_2\text{-}3\text{-epi-D}_3$  in HL60 cellular model.** (A)  $1\alpha,25(\text{OH})_2\text{-}3\text{-epi-D}_3$ -mediated HL60 cell growth.  $1\alpha,25(\text{OH})_2\text{D}_3$  or  $1\alpha,25(\text{OH})_2\text{-}3\text{-epi-D}_3$ -treated HL60 at 1 nM and 100 nM concentrations are counted. Data are presented as mean  $\pm$  S.D. of the mean (\*,  $p < 0.05$ ; \*\*,  $p < 0.01$ ; \*\*\*,  $p < 0.001$ ). (B)  $1\alpha,25(\text{OH})_2\text{-}3\text{-epi-D}_3$ -mediated HL60 cell differentiation into monocyte-like cells. HL60 cells were treated with either ethanol or 1 nM and 100 nM concentration of  $1\alpha,25(\text{OH})_2\text{D}_3$  or  $1\alpha,25(\text{OH})_2\text{-}3\text{-epi-D}_3$ . Cells were labeled with PE-labeled anti-human CD11c and FITC-labeled anti-human CD14, and HL60 cell differentiation was estimated by the double-positive CD11c/CD14 population. Data are representative of three distinct experiments. (PDF)

**Figure S2 Dominant production of the  $1\alpha,25(\text{OH})_2\text{-}3\text{-epi-D}_3$  in keratinocytes after 5 h.** HPLC profile of the CHCl<sub>3</sub>-extract from keratinocytes after 5 h incubation is shown.

### References

- Adorini L, Penna G (2008) Control of autoimmune diseases by the vitamin D endocrine system. *Nat Clin Pract Rheumatol* 4: 404–412.
- Bouillon R, Eelen G, Verlinden L, Mathieu C, Carmeliet G, et al. (2006) Vitamin D and cancer. *J Steroid Biochem Mol Biol* 102: 156–162.
- Pinette KV, Yee YK, Amegadzie BY, Nagpal S (2003) Vitamin D receptor as a drug discovery target. *Mini Rev Med Chem* 3: 193–204.
- Campbell MJ, Adorini L (2006) The vitamin D receptor as a therapeutic target. *Expert Opin Ther Targets* 10: 735–748.
- DeLuca HF (2008) Evolution of our understanding of vitamin D. *Nutr Rev* 66: S73–S87.
- Nagpal S, Na S, Rathnachalam R (2005) Noncalcemic actions of vitamin D receptor ligands. *Endocr Rev* 26: 662–687.
- Garabedian M, Lieberherr M, N'Guyen TM, Corvol MT, Du Bois MB, et al. (1978) The in vitro production and activity of 24, 25-dihydroxycholecalciferol in cartilage and calvarium. *Clin Orthop Relat Res* 135: 241–248.
- Howard GA, Turner RT, Sherrard DJ, Baylink DJ (1981) Human bone cells in culture metabolize 25-hydroxyvitamin D<sub>3</sub> to 1,25-dihydroxyvitamin D<sub>3</sub> and 24,25-dihydroxyvitamin D<sub>3</sub>. *J Biol Chem* 256: 7738–7740.
- Jones G, Vriezien D, Lohnes D, Palda V, Edwards NS (1987) Side-chain hydroxylation of vitamin D<sub>3</sub> and its physiological implications. *Steroids* 49: 29–53.
- Ishizuka S, Norman AW (1987) Metabolic pathways from  $1\alpha,25$ -dihydroxyvitamin D<sub>3</sub> to  $1\alpha,25$ -dihydroxyvitamin D<sub>3</sub>-26,23-lactone. Stereo-retained and stereo-selective lactonization. *J Biol Chem* 262: 7165–7170.
- Bikle DD, Nemanic MK, Whitney JO, Elias PW (1986) Neonatal human foreskin keratinocytes produce 1,25-dihydroxyvitamin D<sub>3</sub>. *Biochemistry* 25: 1545–1548.
- Horst RL (1979) 25-OHD<sub>3</sub>-26,23-lactone: a metabolite of vitamin D<sub>3</sub> that is 5 times more potent than 25-OHD<sub>3</sub> in the rat plasma competitive protein binding radioassay. *Biochem Biophys Res Commun* 89: 286–293.

The amount of  $1\alpha,25(\text{OH})_2\text{-}3\text{-epi-D}_3$  (blue star) is the highest from all the metabolites detected with HPLC. The peak of  $1\alpha,25(\text{OH})_2\text{D}_3$  is highlighted with green star. (PDF)

**Table S1 Data collection and refinement statistics.** (PDF)

**Methods S1 Synthesis.** (PDF)

**Methods S2** (DOCX)

**Scheme S1 Retrosynthesis of 1b.** (PDF)

**Scheme S2 Synthesis of enol triflate 3.** Si = TBS = Si(*t*-Bu)(CH<sub>3</sub>)<sub>2</sub>. TBHP = *t*-BuOOH (a) NaBH<sub>4</sub>, CeCl<sub>3</sub>·7H<sub>2</sub>O, MeOH, 0°C, 30 min. (b) TBHP, VO(acac)<sub>2</sub>, PhH, reflux, 30 min. (c) TBSCl, Im, DMF, rt, 12 h. (d) O<sub>3</sub>, MeOH-CH<sub>2</sub>Cl<sub>2</sub>, -78°C; Ac<sub>2</sub>O, Et<sub>3</sub>N, DMAP, -35°C to -8°C, 2 h; NaOAc, MeOH, 37°C, 12 h. (e) H<sub>3</sub>IO<sub>6</sub>, Et<sub>2</sub>O, rt, 2 h. (f) CBr<sub>4</sub>, Zn, Ph<sub>3</sub>P, CH<sub>2</sub>Cl<sub>2</sub>, rt, 40 min. (g) LDA, THF, -78°C, 1 h; *n*-BuLi, 15 min; 5-Cl-Py-<sub>2</sub>NTf<sub>2</sub>, -78°C to rt, 12 h. (PDF)

**Scheme S3 Synthesis of metabolite 1.** TES = Si(CH<sub>2</sub>CH<sub>3</sub>)<sub>3</sub>. (a) (Ph<sub>3</sub>PCH<sub>2</sub>Br)Br, KO*t*-Bu, toluene, -5°C to rt, 1 h, 80%. (b) TESCl, Im, DMAP, DMF, rt, 3 h, 91%. (c) InCl<sub>3</sub>, *t*-BuLi, THF, -78°C to 0°C, 2 h. (d) 3, (Ph<sub>3</sub>P)<sub>4</sub>Pd, Et<sub>3</sub>N, THF, (dppf)PdCl<sub>2</sub>, 0°C to rt, 12 h. (e) HF·Py, Et<sub>3</sub>N, CH<sub>2</sub>Cl<sub>2</sub>, CH<sub>3</sub>CN, rt, 4 h, 58%. (PDF)

### Acknowledgments

We thank the beam-line staff at the ESRF (Grenoble, France) for help during data collection and T. Huet for critical reading. We thank N. Rouleau and J. Hyvärinen from Perkin Elmer for support in AlphaScreen Assays and V. Prantner for help with statistical analysis.

### Author Contributions

Conceived and designed the experiments: AM DM NR. Performed the experiments: FM RS YS CA IS PA JP. Analyzed the data: FM IS AM NR. Contributed reagents/materials/analysis tools: CM. Wrote the paper: FM AM NR.

13. Wichmann JK, DeLuca HF, Schnoes HK, Horst RL, Shepard RM, et al. (1979) 25-Hydroxyvitamin D $_3$  26,23-lactone: a new in vivo metabolite of vitamin D. *Biochemistry* 18: 4775–4780.
14. DeLuca HF, Suda T, Schnoes HK, Tanaka Y, Holick MF (1970) 25,26-dihydroxycholecalciferol, a metabolite of vitamin D $_3$  with intestinal calcium transport activity. *Biochemistry* 9: 4776–4780.
15. Reinhardt TA, Napoli JL, Pramnik B, Littlelike ET, Beitz DC, et al. (1981) 1 $\alpha$ -25,26-trihydroxyvitamin D $_3$ : an in vivo and in vitro metabolite of vitamin D $_3$ . *Biochemistry* 20: 6230–6235.
16. Holick MF, Schnoes HK, DeLuca HF, Gray RW, Boyle IT, et al. (1972) Isolation and identification of 24,25-dihydroxycholecalciferol, a metabolite of vitamin D made in the kidney. *Biochemistry* 11: 4251–4255.
17. Kumar R, Schnoes HK, DeLuca HF (1978) Rat intestinal 25-hydroxyvitamin D $_3$ - and 1 $\alpha$ ,25-dihydroxyvitamin D $_3$ -24-hydroxylase. *J Biol Chem* 253: 3804–3809.
18. Reddy GS, Rao DS, Siu-Caldera ML, Astecker N, Weiskopf A, et al. (2000) 1 $\alpha$ ,25-dihydroxy-16-ene-23-yne-vitamin D $_3$  and 1 $\alpha$ ,25-dihydroxy-16-ene-23-yne-20-epi-vitamin D $_3$ : analogs of 1 $\alpha$ ,25-dihydroxyvitamin D $_3$  that resist metabolism through the C-24 oxidation pathway are metabolized through the C-3 epimerization pathway. *Arch Biochem Biophys* 383: 197–205.
19. Norman AW, Bouillon R, Farach-Carson MC, Bishop JE, Zhou LX, et al. (1993) Demonstration that 1 beta,25-dihydroxyvitamin D $_3$  is an antagonist of the nongenomic but not genomic biological responses and biological profile of the three A-ring diastereomers of 1 $\alpha$ ,25-dihydroxyvitamin D $_3$ . *J Biol Chem* 268: 20022–20030.
20. Reddy GS, Muralidharan KR, Okamura WH, Tserng K-Y, McLane JA (1994) Metabolism of 1 $\alpha$ ,25-dihydroxyvitamin D $_3$  and one of its A-ring diastereomer 1 $\alpha$ ,25-dihydroxy-3-epi-vitamin D $_3$  in neonatal human keratinocytes. In: Norman AW, Bouillon R, Thomasset M, eds. *Vitamin D a pluripotent steroid hormone: Structural studies, molecular endocrinology and clinical applications*, Walter de Gruyter, NY, USA. Walter de Gruyter, NY, USA. pp 172–173.
21. Reddy GS, Siu-Caldera M-L, Schuster I, Astecker N, Tserng K-Y, et al. (1997) Target tissue specific metabolism of 1 $\alpha$ ,25-dihydroxyvitamin D $_3$  through A-ring modification. In: Norman WA, Bouillon R, Thomasset M, eds. *Vitamin D, chemistry, biology and clinical applications of the steroid hormone*, Riverside, CA, USA. Riverside, CA, USA. pp 139–146.
22. Sekimoto H, Siu-Caldera ML, Weiskopf A, Vouros P, Muralidharan KR, et al. (1999) 1 $\alpha$ ,25-dihydroxy-3-epi-vitamin D $_3$ : in vivo metabolite of 1 $\alpha$ ,25-dihydroxyvitamin D $_3$  in rats. *FEBS Lett* 448: 278–282.
23. Bischof MG, Siu-Caldera ML, Weiskopf A, Vouros P, Cross HS, et al. (1998) Differentiation-related pathways of 1 $\alpha$ ,25-dihydroxycholecalciferol metabolism in human colon adenocarcinoma-derived Caco-2 cells: production of 1 $\alpha$ ,25-dihydroxy-3-epi-cholecalciferol. *Exp Cell Res* 241: 194–201.
24. Rehan VK, Torday JS, Peleg S, Gennaro L, Vouros P, et al. (2002) 1 $\alpha$ ,25-dihydroxy-3-epi-vitamin D $_3$ , a natural metabolite of 1 $\alpha$ ,25-dihydroxy vitamin D $_3$ : production and biological activity studies in pulmonary alveolar type II cells. *Mol Genet Metab* 76: 46–56.
25. Brown AJ, Ritter C, Slatopolsky E, Muralidharan KR, Okamura WH, et al. (1999) 1 $\alpha$ ,25-dihydroxy-3-epi-vitamin D $_3$ , a natural metabolite of 1 $\alpha$ ,25-dihydroxyvitamin D $_3$ , is a potent suppressor of parathyroid hormone secretion. *J Cell Biochem* 73: 106–113.
26. Siu-Caldera ML, Sekimoto H, Weiskopf A, Vouros P, Muralidharan KR, et al. (1999) Production of 1 $\alpha$ ,25-dihydroxy-3-epi-vitamin D $_3$  in two rat osteosarcoma cell lines (UMR 106 and ROS 17/2.8): existence of the C-3 epimerization pathway in ROS 17/2.8 cells in which the C-24 oxidation pathway is not expressed. *Bone* 24: 457–463.
27. Hylemon PB, Sjövall HDAJ (1985) Chapter 12 Metabolism of bile acids in intestinal microflora. In: *New Comprehensive Biochemistry Sterols and Bile Acids* Elsevier. pp 331–343.
28. Penning TM, Bennett MJ, Smith-Hoog S, Schlegel BP, Jez JM, et al. (1997) Structure and function of 3 $\alpha$ -hydroxysteroid dehydrogenase. *Steroids* 62: 101–111.
29. Reddy GS, Rao DS, Siu-Caldera ML (2000) Natural metabolites of 1 $\alpha$ ,25-dihydroxy-vitamin D $_3$  and its analogs. In: Norman AW, Bouillon R, Thomasset, eds. *Vitamin D Endocrine system, Structural, Biological, Genetic and Clinical Aspects*, University of California, Printing and Reprographics, Riverside, CA, USA. pp 139–146.
30. Kamao M, Tatematsu S, Hatakeyama S, Sakaki T, Sawada N, et al. (2004) C-3 epimerization of vitamin D $_3$  metabolites and further metabolism of C-3 epimers: 25-hydroxyvitamin D $_3$  is metabolized to 3-epi-25-hydroxyvitamin D $_3$  and subsequently metabolized through C-1 $\alpha$  or C-24 hydroxylation. *J Biol Chem* 279: 15897–15907.
31. Morrison NA, Eisman JA (1991) Nonhypercalcemic 1,25-(OH) $_2$ D $_3$  analogs potentially induce the human osteocalcin gene promoter stably transfected into rat osteosarcoma cells (ROSCO-2). *J Bone Miner Res* 6: 893–899.
32. Fleet JC, Bradley J, Reddy GS, Ray R, Wood RJ (1996) 1 $\alpha$ ,25-(OH) $_2$ -vitamin D $_3$  analogs with minimal in vivo calcemic activity can stimulate significant transepithelial calcium transport and mRNA expression in vitro. *Arch Biochem Biophys* 329: 228–234.
33. Muralidharan KR, De Lera AR, Isaef SD, Norman AW, Okamura WH (1993) Studies of vitamin D (calciferol) and its analogs. 45. Studies on the A-ring diastereomers of 1 $\alpha$ ,25-dihydroxyvitamin D $_3$ . *J Org Chem* 58: 1895–1899.
34. Gómez-Reino C, Vitale C, Maestro M, Mourinho A (2005) Pd-catalyzed carbocyclization-Negishi cross-coupling cascade: a novel approach to 1 $\alpha$ ,25-dihydroxyvitamin D $_3$  and analogues. *Org Lett* 7: 5885–5887.
35. Zhu G, Okamura WH (1995) Synthesis of Vitamin D (Calciferol). *Chem Rev* 95: 1877–1952.
36. Krause S, Schmalz HG (2000) Palladium-Catalyzed Synthesis of Vitamin D-Active Compounds. In: *Organic Synthesis Highlights IV*. Germany: Wiley and VCH. pp 212–217.
37. Posner GH, Kahraman M (2003) Organic chemistry of vitamin D analogues (deltanoids). *Eur J Org Chem* 2003. pp 3889–3895.
38. Luche JL (1978) Lanthanides in organic chemistry. 1. Selective 1, 2 reductions of conjugated ketones. *J Am Chem Soc* 100: 2226–2227.
39. Sharpless KB, Michaelson RC (1973) High stereo- and regioselectivities in the transition metal catalyzed epoxidations of olefinic alcohols by tert-butyl hydroperoxide. *J Am Chem Soc* 95: 6136–6137.
40. Daniewski AR, Garofalo LM, Hutchings SD, Kabat MM, Liu W, et al. (2002) Efficient synthesis of the A-ring phosphine oxide building block useful for 1 $\alpha$ ,25-dihydroxyvitamin D and analogues. *J Org Chem* 67: 1580–1587.
41. Corey EJ, Fuchs PL (1972) A synthetic method for formyl- $\rightarrow$  ethynyl conversion (RCHO- $\rightarrow$  RCCH or RCCR). *Tetrahedron Lett* 13: 3769–3772.
42. Mourinho A, Torneiro M, Vitale C, Fernández S, Pérez-Sestelo J, et al. (1997) Efficient and versatile synthesis of A-ring precursors of 1 $\alpha$ ,25-dihydroxy-vitamin D $_3$  and analogues. Applications to the synthesis of Lythgoc-Roche phosphine oxide. *Tetrahedron letters* 38: 4713–4716.
43. Gogoi P, Sigüeiro R, Eduardo S, Mourinho A (2010) An expeditious route to 1  $\alpha$ ,25-dihydroxyvitamin D(3) and its analogues by an aqueous tandem palladium-catalyzed a-ring closure and suzuki coupling to the C/D unit. *Eur J Chem* 16: 1432–1435.
44. Trost BM, Dumas J, Villa M (1992) New Strategies for the synthesis of vitamin D metabolites via Pd-catalyzed reactions. *J Am Chem Soc* 114: 9836–9845.
45. Takeyama K, Masuhiro Y, Fuse H, Endoh H, Murayama A, et al. (1999) Selective interaction of vitamin D receptor with transcriptional coactivators by a vitamin D analog. *Mol Cell Biol* 19: 1049–1055.
46. Ullman EF, Kirakossian H, Singh S, Wu ZP, Irvin BR, et al. (1994) Luminescent oxygen channeling immunoassay: measurement of particle binding kinetics by chemiluminescence. *Proc Natl Acad Sci U S A* 91: 5426–5430.
47. Nakagawa K, Sowa Y, Kurobe M, Ozono K, Siu-Caldera ML, et al. (2001) Differential activities of 1 $\alpha$ ,25-dihydroxy-16-ene-vitamin D(3) analogs and their 3-epimers on human promyelocytic leukemia (HL-60) cell differentiation and apoptosis. *Steroids* 66: 327–337.
48. Harant H, Spinner D, Reddy GS, Lindley IJ (2000) Natural metabolites of 1 $\alpha$ ,25-dihydroxyvitamin D(3) retain biological activity mediated through the vitamin D receptor. *J Cell Biochem* 78: 112–120.
49. Rochel N, Wurtz JM, Mitschler A, Klaholz B, Moras D (2000) The crystal structure of the nuclear receptor for vitamin D bound to its natural ligand. *Mol Cell* 5: 173–179.
50. Hourai S, Fujishima T, Kittaka A, Suhara Y, Takayama H, et al. (2006) Probing a water channel near the A-ring of receptor-bound 1  $\alpha$ ,25-dihydroxyvitamin D $_3$  with selected 2 $\alpha$ -substituted analogues. *J Med Chem* 49: 5199–5205.
51. Eelen G, Valle N, Sato Y, Rochel N, Verlinden L, et al. (2008) Superagonistic fluorinated vitamin D $_3$  analogs stabilize helix 12 of the vitamin D receptor. *Chem Biol* 15: 1029–1034.
52. Tocchini-Valentini G, Rochel N, Wurtz JM, Mitschler A, Moras D (2001) Crystal structures of the vitamin D receptor complexed to superagonist 20-epi ligands. *Proc Natl Acad Sci U S A* 98: 5491–5496.
53. Hourai S, Rodrigues LC, Antony P, Reina-San-Martin B, Ciesielski F, et al. (2008) Structure-based design of a superagonist ligand for the vitamin D nuclear receptor. *Chem Biol* 15: 383–392.
54. Rochel N, Tocchini-Valentini G, Egea PF, Juntunen K, Garnier JM, et al. (2001) Functional and structural characterization of the insertion region in the ligand binding domain of the vitamin D nuclear receptor. *Eur J Biochem* 268: 971–979.
55. Molnár F, Peräkylä M, Carlberg C (2006) Vitamin D receptor agonists specifically modulate the volume of the ligand-binding pocket. *J Biol Chem* 281: 10516–10526.
56. Reddy MD, Stoyanova L, Acevedo A, Collins ED (2007) Residues of the human nuclear vitamin D receptor that form hydrogen bonding interactions with the three hydroxyl groups of 1 $\alpha$ ,25-dihydroxyvitamin D $_3$ . *J Steroid Biochem Mol Biol* 103: 347–351.
57. Choi M, Yamamoto K, Masuno H, Nakashima K, Taga T, et al. (2001) Ligand recognition by the vitamin D receptor. *Bioorg Med Chem* 9: 1721–1730.
58. Carlberg C, Bendik I, Wyss A, Meier E, Sturzenbecker LJ, et al. (1993) Two nuclear signalling pathways for vitamin D. *Nature* 361: 657–660.
59. Cormack BP, Valdivia RH, Falkow S (1996) FACS-optimized mutants of the green fluorescent protein (GFP). *Gene* 173: 33–38.
60. Väisänen S, Dunlop TW, Sinkkonen L, Frank C, Carlberg C (2005) Spatio-temporal activation of chromatin on the human CYP24 gene promoter in the presence of 1 $\alpha$ ,25-Dihydroxyvitamin D $_3$ . *J Mol Biol* 350: 65–77.
61. Bligh EG, Dyer WJ (1959) A rapid method of total lipid extraction and purification. *Can J Biochem Physiol* 37: 911–917.
62. Leslie AGW (1992) Recent changes to the MOSFLM package for processing film and image plate data. *Joint CCP4 + ESF-EAMCB Newsletter on Protein Crystallography* No. 26.

63. Murshudov GN, Vagin AA, Dodson EJ (1997) Refinement of macromolecular structures by the maximum-likelihood method. *Acta Crystallogr D Biol Crystallogr* 53: 240–255.
64. Emsley P, Cowtan K (2004) Coot: model-building tools for molecular graphics. *Acta Crystallogr D Biol Crystallogr* 60: 2126–2132.
65. Laskowski RA, MacArthur MW, Moss DS, Thornton JM (1993) PROCHECK: A program to check the stereochemical quality of protein structures. *J Appl Crystallogr* 26: 283–291.